Accepted Manuscript online: 2022-01-03 Article published online: 2022-01-21

Impact of n-Doping Mechanisms on the Molecular Packing and Electron Mobilities of Molecular Semiconductors for Organic Thermoelectrics

Yan Zeng[a,b]
Guangchao Han[a]
Yuanping Yi*[a,b]

[a] Beijing National Laboratory for Molecular Sciences, CAS Key Laboratory of Organic Solids, CAS Research/Education Center for Excellence in Molecular Sciences, Institute of Chemistry, Chinese Academy of Sciences, Beijing 100190, P. R. of China.
[b] University of Chinese Academy of Sciences, Beijing 100049, P. R. of China.
* ypyi@iccas.ac.cn

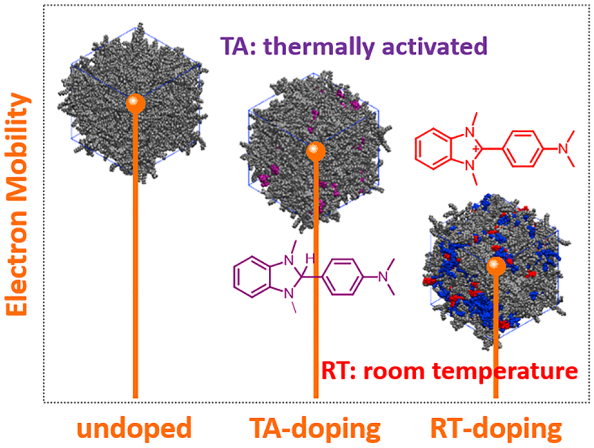

Received: 21.11.2021
Accepted after revision: 30.12.2021
DOI: 10.1055/a-1729-5728; Art ID: OM-2021-11-0042-OA

Abstract Electrical conductivity is one of the key parameters for organic thermoelectrics and depends on both the concentration and mobility of charge carriers. To increase the carrier concentration, molecular dopants have to be added into organic semiconductor materials, whereas the introduction of dopants can influence the molecular packing structures and hence carrier mobility of the organic semiconductors. Herein, we have theoretically investigated the impact of different n-doping mechanisms on molecular packing and electron transport properties by taking (4-(1,3-dimethyl-2,3-dihydro-1H-benzoimidazol-2-yl) phenyl)dimethylamine (N-DMBI-H) and quinoid-dicyanomethylene-dipyrrolo-[3,4-c]pyrrole-1,4-diylidene)bis(thieno[3,2-b]thiophene (Q-DCM-DPPTT) respectively as representative n-dopant and molecular semiconductor. The results show that when the doping reactions and charge transfer spontaneously occur in the solution at room temperature, the oppositely charged dopant and semiconductor molecules will be tightly bound to disrupt the semiconductor to form long-range molecular packing, leading to a substantial decrease of electron mobility in the doped film. In contrast, when the doping reactions and charge transfer are activated by heating the doped film, the molecular packing of the semiconductor is slightly affected and hence the electron mobility remains quite high. This work indicates that thermally activated n-doping is an effective way to achieve both high carrier concentration and high electron mobility in n-type organic thermoelectric materials.

Key words: organic thermoelectric, n-doping mechanisms, molecular packing structure, charge-transport properties

Introduction

Organic semiconductors as potential thermoelectric materials have attracted intense interest owing to the advantages of low cost, ease of fabrication, and light weight.[1–5] An ideal thermoelectric material should possess high Seebeck coefficient, high electrical conductivity, and low thermal conductivity. Organic semiconductors intrinsically have low thermal conductivity and high Seebeck coefficient, but the electrical conductivity is much lower with respect to inorganic semiconductors.[6–10] Therefore, great efforts have been devoted to improving the electrical conductivity to enhance organic thermoelectric performance. Electrical conductivity σ is proportional to carrier concentration n and carrier mobility μ, namely, $\sigma = ne\mu$. Molecular doping is an effective way to increase the carrier concentration in organic semiconductors and hence often adopted to improve the electrical conductivity.[11,12] However, the introduction of molecular dopants can have an important impact on the molecular packing and charge transport in organic semiconductors, and mostly, result in lower carrier mobility.[13–18] Thus, it is critical to reveal how the dopants affect the molecular packing structures of organic semiconductors, especially for n-doping due to the more complicated charge-transfer mechanisms.[19–21]

To achieve efficient n-doping, the electron-donating dopants should have low ionization potentials to facilitate electron transfer from the dopants to semiconductors, making the dopants unstable in the air. Accordingly, air-stable n-dopant precursors have been applied in n-type organic thermoelectric devices. To date, (4-(1,3-dimethyl-2,3-dihydro-1H-benzoimidazol-2-yl)phenyl)dimethylamine (N-DMBI-H, see Figure 1a) is the most successful n-dopant precursor to

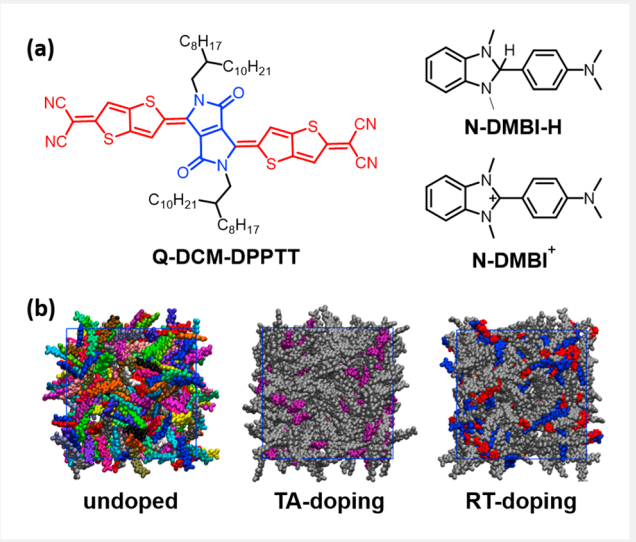

Figure 1 (a) Chemical structures of Q-DCM-DPPTT, N-DMBI-H, and N-DMBI$^+$. The DPP core, TT units, and alkyl side chains in Q-DCM-DPPTT are colored in blue, red, and black, respectively. (b) Illustration of the molecular packing morphologies of undoped, TA-doping and RT-doping films. The side chains are removed for clarity. In the doped films, the neutral Q-DCM-DPPTT, anionic Q-DCM-DPPTT, N-DMBI-H, and N-DMBI$^+$ are colored in silver, blue, purple, and red, respectively.

enhance the carrier concentration and electrical conductivity of n-type organic semiconductors.[4,22–30] To realize n-doping, N-DMBI-H has to undergo a C–H bond cleavage, and the resulting neutral radical N-DMBI· or negative hydride serves as an electron donor.[19,20,22] Interestingly, the C–H bond cleavage reactions depend on the organic semiconductors. For instance, distinct doping mechanisms were found in A-DCV-DPPTT and Q-DCM-DPPTT, two dipyrrolo-[3,4-c] pyrrole-1,4-diylidene)bis(thieno[3,2-b]thiophene (DPPTT) derivatives with aromatic and quinoid structures, respectively (see Figure 1a).[31] In the case of Q-DCM-DPPTT, the doping reactions and charge transfer will occur spontaneously at room temperature upon adding N-DMBI-H into the solution. In contrast, for A-DCV-DPPTT, the doping reactions are inefficient in the solution and activated by heating the doped film. It should be noted that the electrical conductivity of the doped film is over 50 times higher for A-DCV-DPPTT (5.3 S·cm^{-1}) than Q-DCM-DPPTT (0.1 S·cm^{-1}), whereas the electron mobility in the neat film is only 9 times higher for A-DCV-DPPTT than Q-DCM-DPPTT. This implies that the electron mobilities in the doped films are profoundly affected by the different doping mechanisms.

In this contribution, taking N-DMBI-H/Q-DCM-DPPTT as a representative, we have investigated the molecular assembly process and packing morphologies of the neat and doped films by atomistic molecular dynamics (MD) simulations. Moreover, to elucidate the influence of different doping mechanisms, neutral precursor N-DMBI-H and positively charged dopant N-DMBI$^+$ are used during solution processing for thermally activated (TA) and room temperature (RT) doping mechanisms, respectively. In the case of RT doping, a part of Q-DCM-DPPTT molecules are negatively charged to counteract the positive dopants. Based on the obtained thin-film morphologies, electron mobilities are then evaluated in the framework of an incoherent charge hopping and diffusion model. It is found that for RT doping, long-range molecular packing is disrupted by the tight binding between the positive dopant and negative semiconductor molecules, thus substantially decreasing the electron mobility of the doped film. Notably, in the case of TA doping, the molecular packing of the semiconductor is slightly affected by the neutral dopant precursor and the doped film can still exhibit relatively high electron mobility.

Results and Discussion

The molecular assembly processes and the molecular packing morphologies of the formed films are shown in Figure S1 and Figure 1b, respectively. Obviously, before the film formation, the Q-DCM-DPPTT molecules will assemble and pre-aggregate during the solvent evaporation process (Figure S1). It should be noted that when adding the dopants in the solution, the N-DMBI-H molecules tend to be isolated from the semiconductors. However, the cations of N-DMBI$^+$ are close to the anionic Q-DCM-DPPTT molecules to form charge-transfer complexes in the solution. Moreover, because of strong binding energies,[20] these complexes are very stable during the whole solution processing and remain in the doped film (Figure 1b). This means that more contacts between the dopant and semiconductor can be found for the RT doping than for the TA doping.

To further characterize the contacts between the dopant and semiconductor, we calculated the center-of-mass (COM) radial distribution functions (RDFs) of the dopant relative to different parts of Q-DCM-DPPTT, i.e., the DPP core, TT units, and alkyl side chains (see Figure 2a). For both doped films, the RDFs relative to TT show clear peaks at ca. 0.5 nm, whereas no obvious peaks are present in the RDFs relative to DPP and the side chains, indicating that the dopants are inclined to interact with the TT units of Q-DCM-DPPTT (see Figures S2 and S3 for some representative configurations of the dopant/semiconductor complexes). As expected, the peak intensity of the RDF relative to TT is apparently stronger for the RT doping than for the TA doping. In order to quantify the contacts between the dopant and semiconductor, the average number of neighboring Q-DCM-DPPTT molecules for each dopant was calculated according to the shortest interatomic distance between the dopant and semiconductor backbone in the blending films (see Figure 2b). As the threshold distance is increased from 3 to 4 Å, the number of neighbors is dramatically increased, especially N-

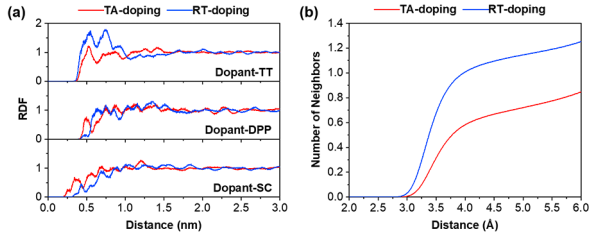

Figure 2 (a) Center-of-mass radial distribution functions of the dopant molecules relative to the DPP core, TT units, and alkyl side chains (SCs) of Q-DCM-DPPTT. (b) Average number of neighbors as a function of the shortest interatomic distance between the dopant molecule and Q-DCM-DPPTT backbone.

DMBI+. At the distance of 4 Å (corresponding to the first shell of neighbors), the number of neighbors reaches ca. 0.6 for N-DMBI-H and even 1.0 for N-DMBI+. The strong interaction between the dopant and Q-DCM-DPPTT is expected to influence the Q-DCM-DPPTT molecular packing, in particular for the RT doping. Furthermore, the dopants are located farther from the Q-DCM-DPPTT in the TA doping film than in the RT doping film, which is beneficial to reduce the Coulomb attraction and increase the chance of charge carriers escaping from the counterions.[32–35]

Figure 3a shows the COM RDFs of the DPP and TT units as well as DPP relative to TT for the neat and doped Q-DCM-DPPTT films. For the DPP-DPP RDFs, no obvious peaks are observed probably due to the large steric hindrance of the out-of-plane alkyl side chains. In sharp contrast, the DPP-TT RDFs display strong peaks at ca. 0.4 nm, which corresponds to typical π–π stacking (see Figure S4). Further, the average number of neighbors was calculated according to the shortest interatomic distance between the Q-DCM-DPPTT backbones (see Figure 3b). We recall that to form a continuous percolation network, each molecule should have at least two neighbors. For the neat film, when the interatomic distance is larger than 3.6 Å, there will be more than two neighbors for each molecule. Compared with the neat film, the doped films exhibit fewer neighbors at the same distance, especially for the RT doping. Consequently, the formation of a percolation network throughout the bulk occurs at a longer distance of ca. 3.8 Å for the TA doping and even ca. 4.3 Å for the RT doping. By and large, the molecular packing is more influenced by the RT doping than by the TA doping.

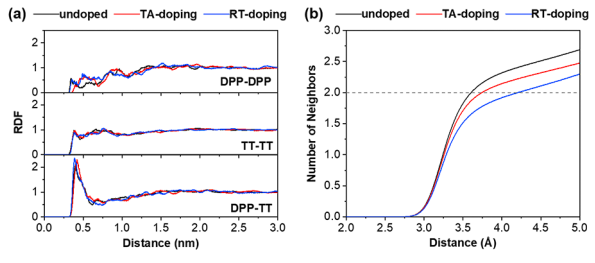

Figure 3 (a) Center-of-mass radial distribution functions of the DPP-DPP, TT-TT, and DPP-TT pairs for Q-DCM-DPPTT. (b) Average number of neighbors as a function of the shortest interatomic distance between the Q-DCM-DPPTT backbones.

To evaluate the influence of molecular packing changes on charge transport in the neat and doped films, we investigated the mesoscopic electrical connection networks that depend on both the number of neighbors and the strength of intermolecular electronic couplings.[36,37] For a given electronic coupling threshold (V_T), we obtained the average number of independent networks (N_{net}) and the average number of Q-DCM-DPPTT molecules in the largest network (N_{max}) of each film (Figure 4). As expected, with increasing V_T, the N_{net} is increased and the N_{max} is decreased. The neat and TA doping films exhibit almost the same N_{net}, which is always smaller than that of the RT doping film. Accordingly, compared with the neat film, the N_{max} is much decreased for the RT doping film while the decrease is relatively small for the TA doping film. For instance, at $V_T = 4$ meV, the largest network contains ca. 40% molecules for the neat film and ca. 30% molecules for the TA doping film, but only ca. 15% molecules for the RT doping film. As illustrated in Figure 4c, the largest connection networks at $V_T = 4$ meV are obviously bigger for the TA doping film than for the RT doping film. Consequently, compared with the neat film, the calculated electron mobility is slightly decreased from 0.021 to 0.017 cm^2/Vs after TA doping, but it is much decreased to 0.009 cm^2/Vs upon RT doping. This implies that the TA dop-

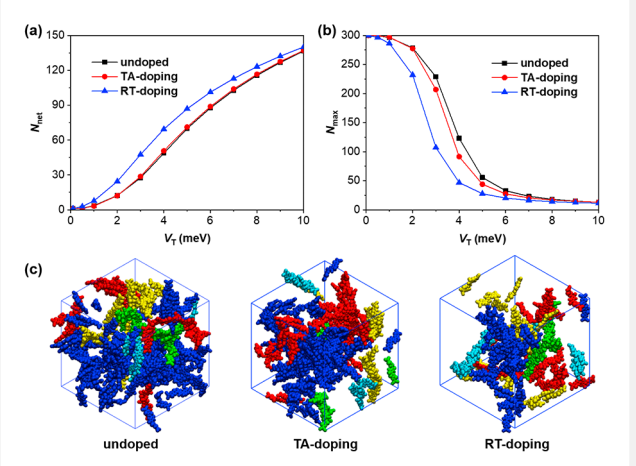

Figure 4 (a) Average number of networks (N_{net}). (b) Average number of molecules in the largest network (N_{max}) as a function of the electronic coupling threshold (V_T). (c) Illustration of the five largest electronic connection networks in different colors at $V_T = 4$ meV.

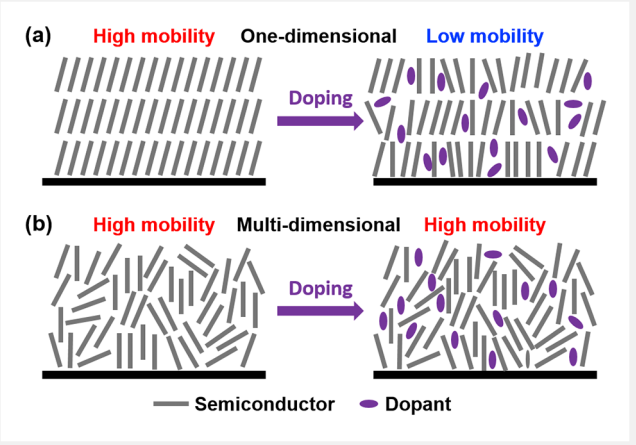

Figure 5 Schematic comparison of the influence of doping on charge transport in the systems with one-dimensional (single crystal) and multi-dimensional (amorphous film) molecular packing structures.

ing is more efficient for improving the electrical conductivity of organic molecular semiconductors.

Here we note that the experimentally measured electron mobility for the neat film (0.07 cm^2/Vs) is more than 3 times higher than our calculated value, but in the case of the doped films, the calculated mobility is relatively higher than the experimental value (0.002 cm^2/Vs). This can be due to the difference between the experimental and simulated molecular packing structures, as illustrated in Figure 5 In reality, the Q-DCM-DPPTT molecules can form one-dimensional long-range and strong π–π stacking due to the high crystallinity nature, but because of the limited simulation conditions (time, size, substrate, etc.), the simulated films show relatively amorphous and isotropic molecular packing structures. Therefore, the experimental mobility is higher than the calculated value for the neat film. After introduction of dopants, the one-dimensional transport channel will be easily interrupted, thus the experimental mobility is substantially decreased in the doped film. In contrast, the doping has a limited impact on the isotropic molecular packing of the simulated amorphous films, and the mobility is less affected upon doping. Therefore, it can be deduced that the organic semiconductors with isotropic transport and high mobility are excellent candidates as doped systems.

Conclusions

We have investigated the impact of different n-doping mechanisms on the molecular packing and charge transport properties of organic semiconductors by taking a representative Q-DCM-DPPTT/N-DMBI-H system. The results point out that because of the steric hindrance of the side chains on the DPP core, the Q-DCM-DPPTT molecules form slipped π–π stacking mainly between the TT terminal and DPP core. Importantly, the dopant is mostly in the vicinity of the TT units instead of the alkyl side chains of Q-DCM-DPPTT in the doped films. Consequently, introduction of the dopants will disrupt the intermolecular percolation network and reduce the carrier mobility. Moreover, because of the formation of strong charge-transfer complexes in solutions, the RT doping results in worse molecular packing and much lower electron mobility with respect to the TA doping. In addition, our work suggests that the influence of molecular doping on charge transport can be minimized in the systems with three-dimensional isotropic molecular packing morphologies.

Experimental Section

Computational methods

The atomistic MD simulations were performed with the Gromacs-4.6.7 package[38] based on the general AMBER force field[39] with the RESP charges.[40] A cut-off of 1.2 nm was applied for the summation of van der Waals interactions and the particle mesh Ewald approach for long-range Coulomb interactions. The isothermal–isobaric (NPT) ensemble was implemented by means of the leap-frog integrator with a time step of 1 fs, and the temperature and pressure were controlled respectively by a velocity rescaling thermostat[41] and Berendsen barostat[42] under three-dimensional periodic boundary conditions.

In order to consider different doping mechanisms, we built three different initial models (undoped, RT doping, and thermally activated doping films) with a large box (25 × 25 × 25 nm) (see the Supporting Information for more details). To make the semiconductor, dopant, and solvent molecules disperse homogeneously and the system relaxed, we ran a 1 ns equilibration under high pressure (100 bar) and then a 20 ns equilibration under normal pressure (1 bar). Next, a quasi-equilibration approach was exploited to simulate solvent evaporation processes by randomly removing 300 solvent molecules every 500 ps from solutions. After removing all solvent molecules, the dried samples were further equilibrated for 30 ns at 1 bar. All the MD simulations were performed at 300 K.

As reported in our previous works, the carrier mobilities of the simulated films were computed within the hopping model based on the semi-classical Marcus theory and kinetic Monte Carlo (KMC) simulations.[43,44] Firstly, the electronic couplings for the effective dimers (in which the average shortest interatomic distance is less than 0.6 nm) were calculated by using Zerner's intermediate neglect of differential overlap method.[45] Then, the electron transfer rates between neighboring semiconductor molecules were estimated by the semi-classical Marcus theory. Finally, based

on the electron-transfer rates and molecular positions, KMC simulations were performed to obtain the carrier hopping trajectories and evaluate the diffusion coefficients and electron mobilities (see the Supporting Information for more details).

Funding Information

The work is supported by the Ministry of Science and Technology of China (Grant No. 2018YFA0703200, 2017YFA0204502) and the National Natural Science Foundation of China (Grant No. 51803216, 51773208, 91833305). MD simulations were carried out on TianHe-1 (A) at the National Supercomputer Center in Tianjin.

Supporting Information

Supporting Information for this article is available online at https://doi.org/10.1055/a-1729-5728.

Conflict of Interest

The authors declare no conflict of interest.

References

(1) Wang, Y.; Yang, L.; Shi, X.-L.; Shi, X.; Chen, L.; Dargusch, M. S.; Zou, J.; Chen, Z.-G. *Adv. Mater.* **2019**, *31*, 1807916.
(2) Russ, B.; Glaudell, A.; Urban, J. J.; Chabinyc, M. L.; Segalman, R. A. *Nat. Rev. Mater.* **2016**, *1*, 16050.
(3) Kroon, R.; Mengistie, D. A.; Kiefer, D.; Hynynen, J.; Ryan, J. D.; Yu, L.; Müller, C. *Chem. Soc. Rev.* **2016**, *45*, 6147.
(4) Sun, Y.; Di, C.-A.; Xu, W.; Zhu, D. *Adv. Electron. Mater.* **2019**, *5*, 1800825.
(5) Deng, L.; Chen, G. *Nano Energy* **2021**, *80*, 105448.
(6) Di, C.-a.; Xu, W.; Zhu, D. *Natl. Sci. Rev.* **2016**, *3*, 269.
(7) Wang, X.; Liman, C. D.; Treat, N. D.; Chabinyc, M. L.; Cahill, D. G. *Phys. Rev. B: Condens. Matter* **2013**, *88*, 075310.
(8) Kim, N.; Domercq, B.; Yoo, S.; Christensen, A.; Kippelen, B.; Graham, S. *Appl. Phys. Lett.* **2005**, *87*, 241908.
(9) Zuo, G.; Liu, X.; Fahlman, M.; Kemerink, M. *Adv. Funct. Mater.* **2017**, *28*, 1703280.
(10) Bubnova, O.; Khan, Z. U.; Wang, H.; Braun, S.; Evans, D. R.; Fabretto, M.; Hojati-Talemi, P.; Dagnelund, D.; Arlin, J.-B.; Geerts, Y. H.; Desbief, S.; Breiby, D. W.; Andreasen, J. W.; Lazzaroni, R.; Chen, W. M.; Zozoulenko, I.; Fahlman, M.; Murphy, P. J.; Berggren, M.; Crispin, X. *Nat. Mater.* **2014**, *13*, 190.
(11) Lüssem, B.; Keum, C.-M.; Kasemann, D.; Naab, B.; Bao, Z.; Leo, K. *Chem. Rev.* **2016**, *116*, 13714.
(12) Lüssem, B.; Riede, M.; Leo, K. *Phys. Status Solidi A* **2013**, *210*, 9.
(13) Xiong, M.; Yan, X.; Li, J.-T.; Zhang, S.; Cao, Z.; Prine, N.; Lu, Y.; Wang, J.-Y.; Gu, X.; Lei, T. *Angew. Chem. Int. Ed.* **2021**, *60*, 8189.
(14) Ma, W.; Shi, K.; Wu, Y.; Lu, Z.-Y.; Liu, H.-Y.; Wang, J.-Y.; Pei, J. *ACS Appl. Mater. Interfaces* **2016**, *8*, 24737.
(15) Yang, C.-Y.; Jin, W.-L.; Wang, J.; Ding, Y.-F.; Nong, S.; Shi, K.; Lu, Y.; Dai, Y.-Z.; Zhuang, F.-D.; Lei, T.; Di, C.-A.; Zhu, D.; Wang, J.-Y.; Pei, J. *Adv. Mater.* **2018**, *30*, 1802850.
(16) Ding, Y.-F.; Yang, C.-Y.; Huang, C.-X.; Lu, Y.; Yao, Z.-F.; Pan, C.-K.; Wang, J.-Y.; Pei, J. *Angew. Chem. Int. Ed.* **2021**, *60*, 5816.
(17) Lu, Y.; Yu, Z.-D.; Un, H.-I.; Yao, Z.-F.; You, H.-Y.; Jin, W.; Li, L.; Wang, Z.-Y.; Dong, B.-W.; Barlow, S.; Longhi, E.; Di, C.-a.; Zhu, D.; Wang, J.-Y.; Silva, C.; Marder, S. R.; Pei, J. *Adv. Mater.* **2021**, *33*, 2005946.
(18) Deng, L.; Huang, X.; Lv, H.; Zhang, Y.; Chen, G. *Appl. Mater. Today* **2021**, *22*, 100959.
(19) Naab, B. D.; Guo, S.; Olthof, S.; Evans, E. G. B.; Wei, P.; Millhauser, G. L.; Kahn, A.; Barlow, S.; Marder, S. R.; Bao, Z. *J. Am. Chem. Soc.* **2013**, *135*, 15018.
(20) Zeng, Y.; Zheng, W.; Guo, Y.; Han, G.; Yi, Y. *J. Mater. Chem. A* **2020**, *8*, 8323.
(21) Schwarze, M.; Naab, B. D.; Tietze, M. L.; Scholz, R.; Pahner, P.; Bussolotti, F.; Kera, S.; Kasemann, D.; Bao, Z.; Leo, K. *ACS Appl. Mater. Interfaces* **2018**, *10*, 1340.
(22) Wei, P.; Oh, J. H.; Dong, G.; Bao, Z. *J. Am. Chem. Soc.* **2010**, *132*, 8852.
(23) Shi, K.; Zhang, F.; Di, C.-A.; Yan, T.-W.; Zou, Y.; Zhou, X.; Zhu, D.; Wang, J.-Y.; Pei, J. *J. Am. Chem. Soc.* **2015**, *137*, 6979.
(24) Liu, J.; Qiu, L.; Portale, G.; Koopmans, M.; ten Brink, G.; Hummelen, J. C.; Koster, L. J. A. *Adv. Mater.* **2017**, *29*, 1701641.
(25) Liu, J.; Qiu, L.; Alessandri, R.; Qiu, X.; Portale, G.; Dong, J.; Talsma, W.; Ye, G.; Sengrian, A. A.; Souza, P. C. T.; Loi, M. A.; Chiechi, R. C.; Marrink, S. J.; Hummelen, J. C.; Koster, L. J. A. *Adv. Mater.* **2018**, *30*, 1704630.
(26) Yuan, D.; Huang, D.; Rivero, S. M.; Carreras, A.; Zhang, C.; Zou, Y.; Jiao, X.; McNeill, C. R.; Zhu, X.; Di, C.-a.; Zhu, D.; Casanova, D.; Casado, J. *Chem* **2019**, *5*, 964.
(27) Dong, C.; Meng, B.; Liu, J.; Wang, L. *ACS Appl. Mater. Interfaces* **2020**, *12*, 10428.
(28) Liu, J.; van der Zee, B.; Alessandri, R.; Sami, S.; Dong, J.; Nugraha, M. I.; Barker, A. J.; Rousseva, S.; Qiu, L.; Qiu, X.; Klasen, N.; Chiechi, R. C.; Baran, D.; Caironi, M.; Anthopoulos, T. D.; Portale, G.; Havenith, R. W. A.; Marrink, S. J.; Hummelen, J. C.; Koster, L. J. A. *Nat. Commun.* **2020**, *11*, 5694.
(29) Feng, K.; Guo, H.; Wang, J.; Shi, Y.; Wu, Z.; Su, M.; Zhang, X.; Son, J. H.; Woo, H. Y.; Guo, X. *J. Am. Chem. Soc.* **2021**, *143*, 1539.
(30) Lu, Y.; Wang, J.-Y.; Pei, J. *Chem. Mater.* **2019**, *31*, 6412.
(31) Huang, D.; Yao, H.; Cui, Y.; Zou, Y.; Zhang, F.; Wang, C.; Shen, H.; Jin, W.; Zhu, J.; Diao, Y.; Xu, W.; Di, C.-a.; Zhu, D. *J. Am. Chem. Soc.* **2017**, *139*, 13013.
(32) Aubry, T. J.; Axtell, J. C.; Basile, V. M.; Winchell, K. J.; Lindemuth, J. R.; Porter, T. M.; Liu, J.-Y.; Alexandrova, A. N.; Kubiak, C. P.; Tolbert, S. H.; Spokoyny, A. M.; Schwartz, B. J. *Adv. Mater.* **2019**, *31*, 1805647.
(33) Liu, J.; Shi, Y.; Dong, J.; Nugraha, M. I.; Qiu, X.; Su, M.; Chiechi, R. C.; Baran, D.; Portale, G.; Guo, X.; Koster, L. J. A. *ACS Energy Lett.* **2019**, *4*, 1556.
(34) Shi, W.; Yildirim, E.; Wu, G.; Wong, Z. M.; Deng, T.; Wang, J.-S.; Xu, J.; Yang, S.-W. *Adv. Theor. Simul.* **2020**, *3*, 2000015.
(35) Shi, W.; Zhao, T.; Xi, J.; Wang, D.; Shuai, Z. *J. Am. Chem. Soc.* **2015**, *137*, 12929.
(36) Savoie, B. M.; Kohlstedt, K. L.; Jackson, N. E.; Chen, L. X.; Olvera de la Cruz, M.; Schatz, G. C.; Marks, T. J.; Ratner, M. A. *Proc. Natl. Acad. Sci. U.S.A.* **2014**, *111*, 10055.
(37) Liu, Y.; Li, M.; Zhou, X.; Jia, Q.-Q.; Feng, S.; Jiang, P.; Xu, X.; Ma, W.; Li, H.-B.; Bo, Z. *ACS Energy Lett.* **2018**, *3*, 1832.

(38) Hess, B.; Kutzner, C.; van der Spoel, D.; Lindahl, E. *J. Chem. Theory Comput.* **2008**, *4*, 435.
(39) Wang, J.; Wolf, R. M.; Caldwell, J. W.; Kollman, P. A.; Case, D. A. *J. Comput. Chem.* **2004**, *25*, 1157.
(40) Bayly, C. I.; Cieplak, P.; Cornell, W.; Kollman, P. A. *J. Phys. Chem.* **1993**, *97*, 10269.
(41) Bussi, G.; Donadio, D.; Parrinello, M. *J. Chem. Phys.* **2007**, *126*, 014101.
(42) Berendsen, H. J. C.; Postma, J. P. M.; van Gunsteren, W. F.; DiNola, A.; Haak, J. R. *J. Chem. Phys.* **1984**, *81*, 3684.
(43) Guo, Y.; Han, G.; Duan, R.; Geng, H.; Yi, Y. *J. Mater. Chem. A* **2018**, *6*, 14224.
(44) Han, G.; Guo, Y.; Song, X.; Wang, Y.; Yi, Y. *J. Mater. Chem. C* **2017**, *5*, 4852.
(45) Ridley, J.; Zerner, M. *Theor. Chim. Acta* **1973**, *32*, 111.